





Active control of jet breakup and droplet formation using temperature modulation

Yavuz Emre Kamis , Huseyin Burak Eral , and Wim-Paul Breugem 
*Delft University of Technology, Department of Process & Energy, Leeghwaterstraat 39,
2628 CM Delft, Netherlands*

 (Received 27 May 2021; accepted 13 October 2021; published 26 October 2021)

Using a slender-jet approach, we numerically investigate the control of jet breakup using temperature modulation at the nozzle with a specified frequency and amplitude. Our results show that temperature modulation does lead to instability through capillary and Marangoni stresses, providing control of the droplet formation in terms of intact length and resultant drop size distribution, which is otherwise irregular due to inevitable presence of background noise. For understanding the mechanisms underpinning the breakup of a thermally modulated jet in the presence of noise, it is useful to decompose the surface tension forces into a contribution from curvature-gradient forces and a contribution from surface tension-gradient forces, associated with axial variations in the jet curvature and the temperature-dependent surface tension coefficient, respectively. We show that in the limit of slow axial heat diffusion and slow cooling to the ambient, as considered here, the breakup of a thermally modulated jet is governed by the ratio of the surface tension-gradient force to the imposed random perturbation force at nozzle exit. This so-called “thermal modulation strength number” depends on the amplitude and frequency of the thermal modulation, the sensitivity of the surface tension coefficient to variations in temperature, the Weber number, and the strength of the Gaussian white noise added to the nozzle exit velocity. We show that the thermal modulation strength number governs the shift in breakup characteristics from forward to rear pinchoff for increasing modulation strength as well as the nature of the instability. When thermal modulation is weak, the surface tension-gradient forces act only as a trigger, and curvature-gradient forces soon take over and grow exponentially downstream from the jet due to inertio-capillary growth. When thermal modulation is strong, the surface tension-gradient forces not only act as a trigger, but remain significant until breakup. The thermal modulation strength number is thus useful to the design of thermal modulation in practical applications as a possible alternative to often-used mechanical excitation mechanisms to control jet breakup.

DOI: [10.1103/PhysRevFluids.6.103903](https://doi.org/10.1103/PhysRevFluids.6.103903)

I. INTRODUCTION

Controlling the formation of droplets from liquid jets is a fundamental challenge whose relevance spans applications at a wide variety of scales, from serial femtosecond x-ray crystallography [1,2], where typical jet lengths are on the order of microns, to production of pharmaceuticals [3,4], where it reaches a few tens of millimeters, and to prilling [5], where the jet lengths typically reach a few tens of centimeters. In all of these applications, understanding and controlling the breakup is essential. The resulting drop size distribution should be predictable, narrow, and monodisperse. If not modulated, it is irregular with a wide distribution. Among the aforementioned applications, control of droplet formation in prilling is particularly challenging and underexplored. Prilling, a commonly used method for production of fertilizers and polymers, is an industrial-scale process

involving breakup of molten polymeric jets and the crystallization of the droplets formed thereafter. From a fluid mechanics and rheology point of view, the challenge in prilling is to control the drop formation of a slender jet with rotational body forces, non-Newtonian effects, and heat transfer.

The study of all processes involving jet breakup starts from the well-known Rayleigh-Plateau instability, which manifests itself as a competition of radii of curvatures on a cylindrical column of liquid. Rayleigh considered the temporal linear stability of an infinite jet in the inviscid limit [6,7]. This was extended by Chandrasekhar by considering the viscous effects [8]. They showed that viscosity slows down the growth and increases the wavelength at which the growth is fastest. In a laboratory frame of reference, however, the instability grows in space as it is convected downstream. Keller *et al.* [9] have performed a spatial analysis and showed that the spatial growth can be approximated by the temporal growth of disturbances on a single thread, provided that the jet speed is sufficiently high, i.e., the downstream motion of a thread has to be much faster than the typical time of capillary growth so the jet can be regarded as infinite. Leib and Goldstein [10] later extended this analysis by accounting for the viscous effects. These studies are from the standpoint of linear stability, where the effects of finite amplitude disturbances cannot be captured. The nonlinear slender-jet model [11–13], based on a Taylor expansion of the radial variable in the governing jet equations, provides a computationally efficient alternative to the linear stability analysis and can be used to cover the whole instability process till breakup. These studies concern a filament in a frame of reference moving with the jet velocity and track the nonlinear evolution using the one-dimensional (1D) slender-jet model. Eggers [11] and Papageorgiou [14,15] considered the 1D slender-jet model close to the breakup and came up with scaling relations to describe the thinning process analytically and showed that the pinch-off process is self-similar. Wilkes *et al.* [16] implemented a two-dimensional (2D) finite element algorithm to study the formation of droplets from a tube, and in a follow-up study, Ambravaneswaran *et al.* [17] discuss the comparison between 1D and 2D models. The main limitation of the 1D model is the inability to capture the overturning of the interface profile very close to the pinchoff when the viscosity is low. However, concerning the balance of inertial, viscous, and capillary forces, the 1D slender-jet model does an excellent job in capturing the nonlinear growth of disturbances in a computationally cheap manner.

When we think of methods to provide a periodic disturbance to a stream, the most commonly encountered methods in the literature are mechanical perturbations, which either perturb the upstream pressure [18] or the orifice of the jet using concentric piezoelements [19,20]. These mechanical perturbations manifest themselves as changes in the local curvature and thus changes in the local Laplace pressure, which leads to instabilities while being advected downstream. A possible alternative to mechanical excitation of the jet is advocated here, which is through thermal modulation of the temperature-dependent surface tension coefficient. Next to perturbations in the capillary stress (Laplace pressure), this also results in an additional stress compared to mechanical excitation: the Marangoni stress related to axial variations in the temperature-dependent surface tension coefficient [21].

The growth of infinitesimal perturbations on nonisothermal jets with thermocapillarity has been studied both analytically and numerically. Xu and Davis [22] performed a linear stability analysis on an infinitely long liquid cylinder subject to a linear temperature gradient. They found that in the limit of high thermal diffusivity and high heat transfer to the ambient, the disturbances vanish and the jet remains stable. Kuhlmann and Rath [23] studied the temporal stability of a liquid bridge bounded by disks at different temperatures and derived marginal stability curves for the critical temperature gradient that would lead to instability. Mashayek and Ashgriz [24] considered nonlinear effects on a nonisothermal thread. Considering a spatially periodic ambient temperature, they identify the critical Biot number at which flows due to capillary pressure and Marangoni stresses cancel out exactly and a stable jet is obtained (i.e., marginal stability). They also study thermal disturbances on the jet surface both with and without surface disturbances. When only thermal disturbances are considered, they report a Marangoni instability and did not observe thermal-capillary instability. Gao and Ng [25] studied the effect of imposed surface tension modulation on a non-Newtonian jet with a Carreau-Yasuda model using slender-jet formulation. Their study does not include the energy

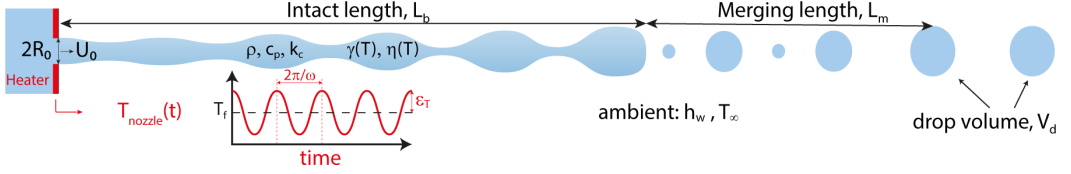


FIG. 1. Illustration of the temperature-controlled jet breakup where the temperature at the nozzle, T_{nozzle} , is modulated to perturb the capillary stress, $\gamma(T)\kappa$, and the Marangoni stress, $\nabla_s \gamma$.

conservation, so the relaxation time of the variations of surface tension cannot be captured. Pillai *et al.* [26] were the first to come up with the nonisothermal slender-jet equations. They studied velocity modulations on a slender jet with temperature-dependent surface tension and viscosity, and subject to cooling. Faidley and Panton [27] carried out the first experiments to test the idea of thermal modulation at the nozzle. They reported agreement with Rayleigh's dispersion relation for an isothermal jet. However, at very high and low wave numbers the background noise dominated over the colored perturbations, since the growth rates at both limits are very low. The idea of using thermally induced perturbations to control jet breakup drew attention in studies of continuous ink jet printing also [28]. Heating elements at the inlet have also been studied and utilized for alternative purposes as well. Chwalek *et al.* [29] used asymmetric heating at the nozzle inlet as a method to deflect microjets. Suryo and Basaran [30] numerically studied a pendant drop and demonstrated that dripping can occur even in the absence of gravity by means of a line heater located at the inlet.

Nonisothermal jet breakup bears many analogies with surfactant-laden jet breakup. The presence of Marangoni stress in this case is due to the variation of surfactant concentration on the jet interface that gives rise to gradients in the surface tension coefficient. Ambravaneswaran *et al.* [31] extended the 1D slender-jet equations in the presence of soluble surfactants to consider the effect of Marangoni stress on the evolution of instabilities. Kamat *et al.* [32] showed that the presence of surfactants may give rise to formation of a sequence of microthreads close to the pinchoff, which is not seen in surfactant-free threads. Wee *et al.* [33] considered a viscous thread in the presence of surfactants and derived a scaling relation that would make it possible to measure the surface viscosity of a surfactant-laden drop by using the temporal evolution of the neck thickness.

An analysis of the spatial development and nonlinear breakup of a temperature-modulated jet has not been reported yet in literature. To this purpose we have employed the slender-jet model in the present study. Our objective is to gain insight in the underlying physical mechanisms responsible for the initiation and breakup of a straight and Newtonian jet that is thermally modulated at nozzle exit. We developed a 1D model within the framework of a slender-jet approximation and studied the nonlinear spatial instabilities due to the thermal modulation. The selected parameter space is motivated by typical conditions in prilling applications. We studied the effects of the thermal modulation characteristics (frequency and amplitude) as well as the thermal sensitivity of the surface tension coefficient on breakup and the droplet size distribution.

II. MATHEMATICAL BACKGROUND

The mass conservation, Cauchy momentum, and energy equations for the case described in Fig. 1 are as follows:

$$\nabla \cdot \mathbf{v} = 0, \quad (1a)$$

$$\rho \left(\frac{\partial \mathbf{v}}{\partial t} + (\mathbf{v} \cdot \nabla) \mathbf{v} \right) = \nabla \cdot \boldsymbol{\sigma}, \quad (1b)$$

$$\rho c_p \left(\frac{\partial T}{\partial t} + (\mathbf{v} \cdot \nabla) T \right) = k_c \nabla^2 T, \quad (1c)$$

where the total stress tensor for a Newtonian fluid is defined as $\boldsymbol{\sigma} = -p\mathbf{I} + 2\eta(T)\mathbf{D}$ and $2\mathbf{D} = \nabla\mathbf{v} + (\nabla\mathbf{v})^T$. Here, ρ , c_p , and k_c represent the density, specific heat capacity, and the thermal conductivity of the liquid, respectively.

On the free surface one has the continuity of normal and tangential stresses, i.e., the dynamic boundary condition:

$$\boldsymbol{\sigma} \cdot \mathbf{n} = -\gamma(T)\kappa\mathbf{n} + \nabla_s\gamma(T), \quad (2)$$

where \mathbf{n} is the outward unit normal, $\nabla_s = (\mathbf{I} - \mathbf{nn}) \cdot \nabla$ is the surface gradient operator, and $\kappa = \nabla_s \cdot \mathbf{n}$ is the curvature of the free surface, respectively. The constitutive relations for temperature-dependent surface tension and viscosity are approximated as

$$\gamma(T) = \gamma_0 - \beta(T - T_m), \quad (3a)$$

$$\eta(T) = \eta_0 \exp[-\alpha(T - T_m)], \quad (3b)$$

where $\beta[\text{N m}^{-1} \text{K}^{-1}]$ is the first-order temperature dependency of surface tension (i.e., $d\gamma/dT = -\beta$) and $\alpha[\text{K}^{-1}]$ is a positive constant representing how rapidly viscosity changes with temperature.

In addition to the dynamic boundary condition, one has the kinematic boundary condition of the jet interface at $r = R(z, t)$ moving with the local radial velocity:

$$\frac{\partial R}{\partial t} + v \frac{\partial R}{\partial z} = u|_{r=R(z,t)}. \quad (4)$$

And finally, one has the heat transfer at the interface, given by

$$-k_c\mathbf{n} \cdot \nabla T = h_w(T - T_\infty), \quad (5)$$

where h_w is the heat transfer coefficient between the liquid jet and the ambient, which is at a temperature of T_∞ .

Here we adopt the slender-jet approximation for an axisymmetric jet [12], in which it is assumed that the radial variations are much weaker than axial variations in the velocity, pressure, and temperature. This forms the basis for a Taylor series expansion of the flow variables in r :

$$\begin{aligned} v(z, r, t) &= v_0(z, t) + v_2(z, t)r^2 + \dots, \\ u(z, r, t) &= -\frac{1}{2}v_0'(z, t)r - \frac{1}{4}v_2'(z, t)r^3 - \dots, \\ p(z, r, t) &= p_0(z, t) + p_2(z, t)r^2 + \dots, \\ T(z, r, t) &= T_0(z, t) + T_2(z, t)r^2 + \dots, \end{aligned} \quad (6)$$

where primes denote $\frac{\partial}{\partial z}$. Inserting (6) in (1)–(5) and keeping only the terms that are leading order in r will yield the nonisothermal slender-jet equations

$$\frac{\partial R^2}{\partial t} + (vR^2)' = 0, \quad (7a)$$

$$\rho \left(\frac{\partial v}{\partial t} + vv' \right) = -(\gamma(T)\kappa)' + \frac{\partial \gamma}{\partial T} T' \frac{2}{R} + 3\eta(T) \frac{(v'R^2)'}{R^2} + 3 \frac{\partial \eta}{\partial T} T' v', \quad (7b)$$

$$\rho c_p \left(\frac{\partial T}{\partial t} + vT' \right) = k_c \left(T'' + \frac{2T'R'}{R} - \frac{2h_w(T - T_\infty)}{k_c R} \right), \quad (7c)$$

where κ is the curvature, given by

$$\kappa = \frac{1}{\sqrt{1 + R^2}} \left(\frac{1}{R} - \frac{R''}{1 + R^2} \right). \quad (8)$$

Some details of the derivation regarding the interface conditions are discussed in Appendix A.

The problem at hand is a multiphysics problem where capillary, thermocapillary, inertial, convective, and diffusive (both for momentum and energy) events take place simultaneously. So it is convenient to list the relevant timescales that result from the balance of these events before nondimensionalization:

$$\begin{aligned}
 t_{IC} &= \sqrt{\frac{\rho R_0^3}{\gamma_0}} = \text{Inertio-capillary timescale,} \\
 t_{ITC} &= \sqrt{\frac{\rho R_0^3}{\beta \Delta T}} = \text{Inertio-thermocapillary timescale,} \\
 t_{VC} &= \frac{\eta_0 R_0}{\gamma_0} = \text{Visco-capillary timescale,} \\
 t_A &= \frac{R_0}{U_0} = \text{Advection timescale,} \\
 t_{TVC} &= \frac{\alpha \Delta T \eta_0 R_0}{\gamma_0} = \text{Thermo-visco-capillary timescale,} \\
 t_{TD} &= \frac{R_0^2 \rho c_p}{k_c} = \text{Thermal diffusive timescale,} \\
 t_{TC} &= \frac{\rho c_p R_0}{h_w} = \text{Thermal cooling timescale.}
 \end{aligned} \tag{9}$$

These seven timescales will yield six nondimensional numbers, namely,

$$\begin{aligned}
 \text{We} &= \frac{t_{IC}^2}{t_A^2}, \quad \text{Ca} = \frac{t_{VC}}{t_A}, \quad \text{Pe} = \frac{t_{TD}}{t_A} \\
 \text{Bi} &= \frac{t_{TD}}{t_{TC}}, \quad \Pi_\gamma = \frac{t_{IC}^2}{t_{ITC}^2}, \quad \Pi_\eta = \frac{t_{TVC}}{t_{VC}}.
 \end{aligned} \tag{10}$$

To make the system nondimensional, all spatial variables are expressed in units of R_0 , all velocities in units of U_0 , so nondimensional time is expressed in units of advection time $t_A = R_0/U_0$. The characteristic stress is given by capillary stress, γ_0/R_0 , and the nondimensional temperature is expressed as

$$\Theta(z, t) = \frac{T(z, t) - T_m}{\Delta T}, \tag{11}$$

with $\Delta T = T_f - T_m$, where T_m is the melting point of the molten jet, and T_f is the feed temperature of the jet. Hence, $\Theta = 0$ at the melting point, $\Theta = 1$ at the feed temperature, which is also the inlet temperature, and finally, $\Theta = \Theta_\infty < 0$ for the ambient temperature. Using these characteristics and with the definitions of the nondimensional numbers given in (10), the nondimensional set of governing equations is as follows:

$$\frac{\partial R^2}{\partial t} + \frac{\partial v R^2}{\partial z} = 0, \tag{12a}$$

$$\frac{\partial v R^2}{\partial t} + \frac{\partial v^2 R^2}{\partial z} = \frac{1}{\text{We}} \frac{\partial}{\partial z} [R^2 (\tau_\gamma + \tau_\eta)] - \frac{\Pi_\gamma 2R}{\text{We}} \left(1 - \frac{1}{\sqrt{1 + R^2}} \right) \frac{\partial \Theta}{\partial z}, \tag{12b}$$

$$\frac{\partial R^2 \Theta}{\partial t} + \frac{\partial (v R^2 \Theta)}{\partial z} = \frac{1}{\text{Pe}} \frac{\partial}{\partial z} \left(R^2 \frac{\partial \Theta}{\partial z} \right) - \frac{2\text{Bi} R}{\text{Pe}} (\Theta - \Theta_\infty), \tag{12c}$$

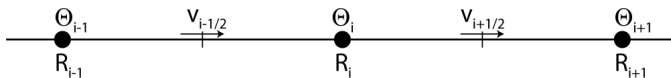


FIG. 2. A schematic of the staggered grid.

where τ_γ and τ_η are the capillary and viscous stresses integrated over the cross-sectional area, given by

$$\tau_\gamma = \gamma(\Theta)K, \quad \tau_\eta = 3Ca\eta(\Theta)\frac{\partial v}{\partial z},$$

$$K = \frac{1}{\sqrt{1+R'^2}} \left(\frac{1}{R} + \frac{R''}{1+R'^2} \right).$$

Finally, the nondimensional form of the temperature-dependent material properties becomes

$$\gamma(\Theta) = 1 - \Pi_\gamma \Theta, \quad (13a)$$

$$\eta(\Theta) = \exp(-\alpha \Delta T \Theta). \quad (13b)$$

The resulting system of 1D unsteady equations (12) and (13) is solved for the conserved variables R^2 , vR^2 , and ΘR^2 . We use a finite-difference scheme on a staggered grid where the jet cross section and the temperatures are stored in cell centers, and the velocities are stored on cell faces, as shown in Fig. 2. The jet domain spans $z \in [0, L]$ where $L = 300R_0$, with the following initial and boundary conditions:

$$\begin{aligned} R^2(0, t) &= 1, & vR^2(0, t) &= 1 + W(t), \\ \Theta R^2(0, t) &= 1 + \varepsilon_T \sin \omega t, \\ R^2(z, 0) &= vR^2(z, 0) = \Theta R^2(z, 0) = 1, \end{aligned} \quad (14)$$

where $W(t)$ is a Gaussian white noise term added on the jet velocity, which is described in Sec. III A. ε_T and ω represent the amplitude and the frequency of the temperature modulation at the inlet. On the downstream end of the domain, a convective open boundary condition is used [34]. The time integration is done explicitly by a three-step Runge-Kutta scheme with adaptive time stepping. Except for velocities, a central differencing scheme is used for evaluating the variables at their half step neighbors, but for velocities a higher-order total variation diminishing (TVD) van Leer scheme is used [35]. The singularity at pinchoff is regularized in a similar fashion described in [36], so that the drop formation and merging phenomena can also be accounted for. In this scheme, a sufficiently small (on the order of the grid size) cutoff radius, R_c , is selected beyond which the jet does not thin further. Its effects vanish with smaller grid size. Grid independence studies were carried out, and we validated that the regularization does not affect the breakup time nor the dynamics of the droplets that are formed. In figures that show the jet shape (Figs. 4 and 7), only the parts where $R > R_c$ are shown to avoid confusion with the beads-on-a-string structure seen in viscoelastic liquids [37]. In Appendix B we briefly discuss some benchmark studies using our code with respect to 1D- and 2D-axisymmetric cases from the literature.

III. RESULTS AND DISCUSSION

A. Natural breakup of a nonisothermal jet under cooling

The fate of an uncontrolled jet is an challenging topic on its own and has been addressed experimentally and theoretically [38–40]. In their recent work, Ganán-Calvo *et al.* [39] propose a universal scaling law from a time-averaged energy balance of the steady flow of an isothermal jet and the perturbations thereon, and use experiments and simulations to determine the universal fitting constants. In the framework of the slender-jet approximation, an isothermal jet will remain stable

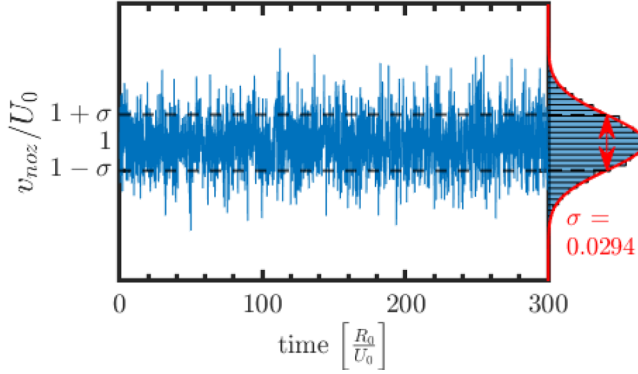


FIG. 3. Random velocity fluctuations imposed at the nozzle, the standard deviation σ scales with $A\Delta t$, where Δt is the adaptive time step, and A is a free constant that adjusts the strength of the fluctuation.

(provided that external body forces are negligible and $We > We_c$) if no perturbation is numerically imposed. So to set the reference case of an uncontrolled jet, we consider a jet with a Gaussian white noise added on top of the nozzle exit velocity, as shown in Fig. 3, with a standard deviation of $A\Delta t$, where A is a free parameter to set the strength of the noise. So the forcing (per unit volume) by the random velocity fluctuation at the nozzle scales as $\rho(\partial v/\partial t)_{\text{noz}} \sim \rho U_0^2 A/R_0$ in dimensional units. This way of implementing the random noise makes sure that the forcing that results from the random fluctuations are uncorrelated with the time discretizations as desired. The strength parameter A is adjusted such that the intact length is in agreement with the experimental scaling law for the natural breakup of Newtonian jets [39] and fixed at a value of $A = 40$ in all of the simulations.

In the presence of ambient cooling, the stationary profiles of temperature and the radius of the jet will also be nonuniform. If the cooling rate is strong enough, the Marangoni stresses due to the base state temperature profile will significantly accelerate the jet and lead to breakup (even without background noise), analogous to gravity-driven jets [41].

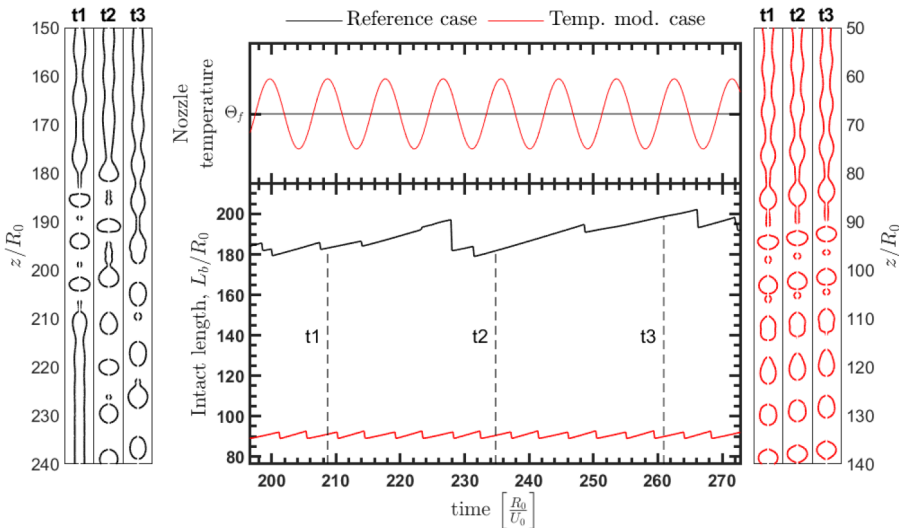


FIG. 4. A comparison of the isothermal reference case (black) and a temperature-modulated case (red) for $\varepsilon_T = 0.05$, $\Pi_\gamma = 0.05$, and $\omega = 0.7$. Parts of the jet where $R < R_c$ are not shown to avoid confusion with the beads-on-a-string structure seen in viscoelastic liquids.

TABLE I. Fluid properties for molten urea [42] and the operating conditions for a typical prilling process [5] used in the simulations.

Fluid properties, Urea @ 135 °C	
Melting point	$T_m \approx 133 \text{ °C}$
Density	$\rho \approx 1247 \text{ kg m}^{-3}$
Dynamic viscosity	$\eta_0 \approx 3 \text{ mPa s}$
Surface tension	$\gamma_0 \approx 66 \text{ mN M}^{-1}$
Specific heat capacity	$c_p \approx 2.25 \text{ kJkg}^{-1} \text{ K}^{-1}$
Thermal conductivity	$k_c \approx 1.2 \text{ W.m}^{-1} \text{ K}^{-1}$
Thermal sensitivity of viscosity	$\alpha \approx 0.02 \text{ K}^{-1}$
Typical process conditions	
Orifice radius	$R_0 \approx 700 \text{ }\mu\text{m}$
Jet velocity	$U_0 \approx 1 \text{ m s}^{-1}$
Feed temperature	$T_f \approx 145 \text{ °C}$
Ambient temperature	$T_\infty > 25 \text{ °C}$
Heat transfer coefficient	$h_w \approx 0.86 \text{ W m}^{-2} \text{ K}^{-1}$

In the absence of the temperature modulation at the inlet, the jet is only perturbed by the white noise, that is, the random velocity fluctuations at the inlet. This means the perturbation has a spectrum of frequencies without a dominant amplitude at any frequency, so the breakup will consist of various frequencies superposed onto each other. The result is an irregular variation of the jet intact length, which is the distance from the inlet to the point of the first breakup. Figure 4 shows the variation of the intact length over time for a jet that is only perturbed by the white noise (from here on referred to as the reference case).

B. Temperature modulation at the inlet

The metrics of the control of jet breakup and droplet formation can be described in two facets: (1) Controlling the intact length, and hence controlling where the droplet formation takes place, and (2) controlling the mean and spread of the drop size distribution. The choices of the nondimensional numbers in our simulations are motivated by typical conditions for a molten urea jet in a prilling process [5,42], which are listed in Table I.

Based on this we fixed five of the six nondimensional numbers given in (10): $We = 50$, $Ca = 0.21$, $Pe = 1320$, $Bi = 0.5$, and $\Pi_\eta = 0.1$, as well as $\Theta_\infty = -4$, in all of our simulations. We varied Π_γ , i.e., the nondimensional form of the temperature sensitivity of the surface tension coefficient, between $\Pi_\gamma \in [0.005, 0.5]$ (with a typical value of 0.5 for urea). Furthermore, we also studied $\varepsilon_T \in [0.005, 0.5]$ as modulation amplitude and $\omega \in [0.1, 1.2]$ as modulation frequency, respectively.

Figure 4 lays out an overall comparison between the reference case which has no temperature modulation and a modulated case with $\varepsilon_T = 0.05$, $\omega = 0.7$, and $\Pi_\gamma = 0.05$. It shows that when a temperature modulation is introduced on top of the noise, the time series for the intact length changes significantly, where the intact length is defined as the length measured from the nozzle exit over which the jet remains intact (see Fig. 1). The mean intact length gets shorter and the irregularity due to the noise is suppressed, thanks to the finite amplitude perturbation that is imposed. The variance of the intact length of the temperature-modulated jet shows more of a periodic trend. When we look at the shape of the jet at several instants, they show recurrence and hence better control in terms of predictability of the location of the generated droplet stream.

Figure 5 shows how the intact length changes with respect to the modulation frequencies. The results are in agreement with the presented results of nonlinear temporal analysis of a nonisothermal thread [24], since the Weber number in the simulations here is above the critical Weber number

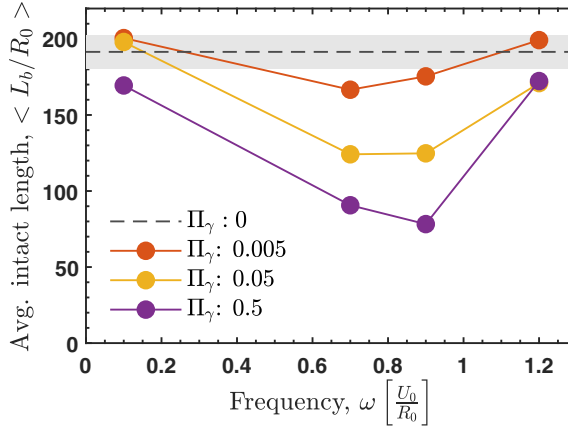


FIG. 5. The intact length as a function of modulation frequency and Π_γ ; the temperature modulation amplitude is fixed at $\varepsilon_T = 0.05$. The gray shaded region covers one standard deviation above and below the mean intact length for the reference case (i.e., $\Pi_\gamma = 0$).

[9,10]. The frequency at which the fastest growth takes place (i.e., shortest L_b) increases slightly with increasing Π_γ .

A more quantitative comparison of the drops generated from the two cases can be obtained from Fig. 6. Each of the sharp drops in the intact length seen in Fig. 4 represents a droplet that is generated at the tip of the jet. For the temperature-modulated case, the size distribution of the droplets generated at the tip of the stream is bimodal, namely, there is a periodic generation of a main droplet followed by a satellite droplet whose volume ratio is governed by the perturbation frequency. The satellite and the main drops merge after a certain distance downstream from the point where they are generated, as shown in Fig. 4. Whether the satellite drops merge with the main drop that precedes or succeeds it depends on the location of the pinchoff within a single filament [43,44]. The changes in the average drop sizes with respect to the frequency of modulation at the inlet is given in Table II. Note that the thermal modulation is not sufficiently strong to control jet breakup at the lowest frequency ($\omega = 0.1$), which is also evident from Fig. 5; the modulation is overwhelmed here by the presence of noise.

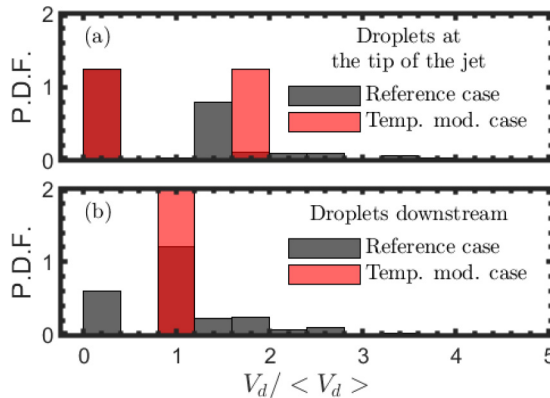


FIG. 6. Comparison of the drop size distributions of the isothermal reference case and temperature-modulated case shown in Fig. 4: (a) at the tip of the intact jet, $z = L_b$, and (b) downstream, $z = 280R_0$. The parameters for the perturbed case are $\varepsilon_T = 0.5$, $\omega = 0.7$, and $\Pi_\gamma = 0.05$.

TABLE II. Average drop volumes with respect to the frequency of perturbation at the inlet. The model parameters are $\varepsilon_T = 0.05$ and $\Pi_\gamma = 0.05$.

Average drop volumes, normalized by R_0^3		
Frequency at the inlet ω	Avg. drop volume $\langle V_d \rangle$	Volume of a single thread $\pi R_0^2 \lambda \approx \pi R_0^2 U_0 \frac{2\pi}{\omega}$
0.1	29.05	197.4
0.7	27.57	28.20
0.9	21.01	21.93
1.2	17.23	16.45

For isothermal jets, the shift in the pinch-off character is dependant on the amplitude of the modulation where the rear pinchoff only occurs in a narrow window of amplitudes [44]. In the case studied here, the modulation comes from a superposition of temperature modulation and random velocity fluctuations at the nozzle exit. The temperature modulation is coupled to the liquid through the nondimensional number, Π_γ , which measures the sensitivity of surface tension to changes in temperature. Figure 7 shows the variation of the time-averaged intact length and merging length of the jet. The merging length is defined from the tip of the jet where $z = L_b$ to the point where uniform droplets are formed ($z = L_b + L_m$), as shown in Fig. 1. As expected, for stronger modulations on the surface tension coefficient (i.e., higher $\Pi_\gamma \varepsilon_T$), the average intact length decays. The pinch-off character also shifts from forward to rear pinching.

For gaining physical understanding, it is useful to identify the important forces and how they scale. The case studied here is motivated by a typical process, where $Pe = 1320$ and $Bi = 0.5$ are fixed parameters. The large Pe and small Bi suggest that diffusion of heat within the jet and loss of heat to the ambient are negligible (though they are included in the computations). So the problem can be narrowed down to the competition of forcing due to background noise, $f_{bg} \sim \rho(\partial v/\partial z)_{noz} \sim \rho U_0^2 A/R_0$, and forcing due to temperature modulation, $f_{tm} \sim (1/R_0)(\partial \gamma/\partial z)_{noz} \sim \Pi_\gamma \varepsilon_T \omega \gamma_0/R_0^2$. Their ratio can be written as a nondimensional ‘‘thermal modulation strength number,’’ \mathcal{M} ,

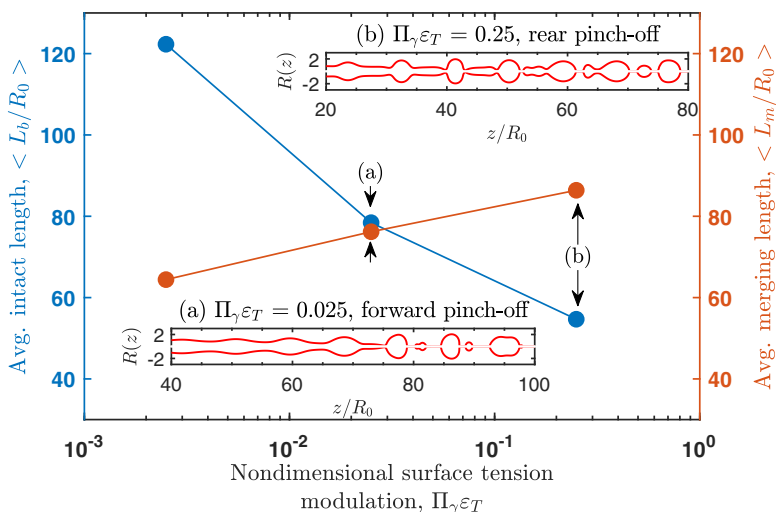


FIG. 7. Average intact and merging lengths of the jet with respect to the modulation on the surface tension coefficient for $\omega = 0.7$. Insets show the two cases where the pinch-off characteristic shifts from (a) forward pinchoff to (b) rear pinchoff.

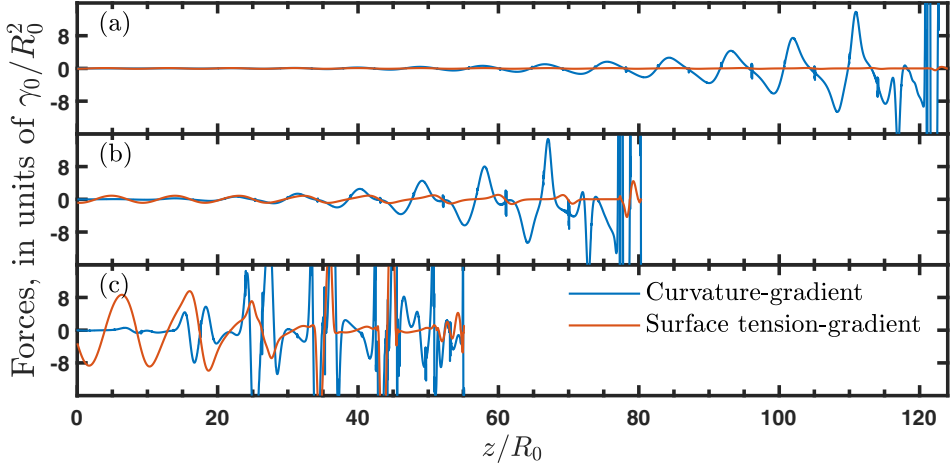


FIG. 8. Growth of the stress perturbations for different surface tension sensitivities: (a) $\Pi_\gamma \varepsilon_T = 0.0025$, (b) $\Pi_\gamma \varepsilon_T = 0.025$, and (c) $\Pi_\gamma \varepsilon_T = 0.25$. The modulation frequency, ω , is fixed at 0.7.

defined as

$$\mathcal{M} = \frac{f_{im}}{f_{bg}} \sim \frac{\Pi_\gamma \varepsilon_T \omega}{\text{We} A}. \quad (15)$$

This also explains the discrepancy between the average drop volume and the volume of a single thread for the low frequency in Table II. Except for $\omega = 0.1$, the frequency of temperature modulation dictates the average drop volumes, but in the case $\omega = 0.1$, the instability due to temperature modulation grows slower than that of background noise and the average drop size is dictated by the random background noise, which is closer to the value that is obtained at the fastest-growing frequency.

The modulation in temperature yields two disturbance mechanisms that are out of phase with each other. The first one is due to the local change in surface tension coefficient, which manifests itself as an axial variation in the capillary pressure. Cold regions correspond to a higher surface tension coefficient and hence a higher capillary pressure at similar curvature, which thus tends to drive the flow from cold to hot regions. The second one originates from the gradient of surface tension coefficient along the jet, which gives rise to Marangoni stresses that drive the flow from regions of low to high surface tension coefficient, i.e., from hot to cold regions. The surface tension forces in the flow, f_{st} , can be grouped as follows:

$$f_{st} = \underbrace{-\gamma \frac{\partial \kappa}{\partial z}}_{\text{curvature gradient}} + \underbrace{\left(\frac{2}{R} - \kappa\right) \frac{\partial \gamma}{\partial z}}_{\text{surface tension gradient}}. \quad (16)$$

If there is no surface perturbation initially, the gradient of the curvature is zero and the forcing comes only from the terms related to the gradient of the surface tension coefficient [second term on the RHS of Eq. (16)]. The magnitude of the force is higher for higher $\Pi_\gamma \varepsilon_T \omega$ [see Eq. (15)], which is the amplitude of the stress perturbations, given in Fig. 8. This is the reason for the shift in pinch-off character shown in Fig. 7, namely, even though the amplitudes of temperature modulation at the nozzle are identical for both cases, the amplitudes of the corresponding stress perturbations are an order of magnitude different due to the different Π_γ values. This stress variation with a magnitude of $\Pi_\gamma \varepsilon_T \omega$ leads to surface variations later downstream, and then a combination of capillary and Marangoni stresses act on the jet. In the cases where heat diffusion is also significant (i.e., low Péclet

number), for instance, with liquid metal jets, the temperature will tend to unify along the jet and the gradient of the surface tension coefficient would disappear, making the curvature effects the only driving force for the instability. The case studied here is at a high Péclet number, so the disturbances due to temperature gradient remain finite. Their significance with respect to the capillary growth depends on the value of $\Pi_\gamma \varepsilon_T$ (for fixed We , A , and ω). From Fig. 8 one can identify three different regimes. When $\Pi_\gamma \varepsilon_T$ is low [in Fig. 8(a)], the background noise is in charge of the instability that leads to breakup and the amplitude of the curvature-gradient forces grows exponentially. With a moderate value of $\Pi_\gamma \varepsilon_T$ [in Fig. 8(b)], the temperature modulation acts as a finite amplitude disturbance to initiate the capillary breakup, in other words, it triggers the capillary breakup of the jet with a shorter intact length. The curvature forces start to grow close to the nozzle with a phase difference with respect to the surface tension-gradient forces, then take over the process and grow exponentially. And finally, at high values of $\Pi_\gamma \varepsilon_T$ [in Fig. 8(c)] the surface tension-gradient forces are hindering the exponential growth of curvature forces and remain on the same order of magnitude until the breakup, which is even shorter due to the higher amplitude of forcing at the nozzle.

IV. CONCLUSION

We numerically demonstrate that modulating the inlet temperature of straight jets can be used for controlling the breakup and formation of the droplets. The temperature modulation manifests itself as local perturbations in thermally induced capillary and Marangoni stresses. For deeper physical understanding we proposed to decompose the surface tension forces into a contribution from curvature-gradient and surface tension-gradient forces. The ratio of the surface-tension-gradient force to the imposed random perturbation force at the nozzle exit can be expressed by the so-called thermal modulation strength number, \mathcal{M} . This number depends on the amplitude and frequency of the thermal modulation and the sensitivity of surface tension to variations in temperature on the one hand, and the Weber number and noise amplitude in the nozzle exit velocity on the other hand, as expressed by Eq. (15). Larger values of the thermal modulation strength number provide a better control, shorter intact lengths, and more uniform droplet streams. Correspondingly, with increasing modulation strength, the role of thermal modulation shifts from being only a trigger for exponential growth of curvature-gradient forces to the case where both curvature-gradient and surface tension-gradient forces are dominant until pinchoff. The thermal modulation strength number is thus a useful criterion to the design of thermal modulation for controlled jet breakup in practice, in particular for determining the minimal required thermal modulation strength for generating a uniform droplet stream. Natural extensions of the present work are case studies of thermal modulation in the presence of non-negligible axial heat conduction and/or cooling to the ambient.

ACKNOWLEDGMENTS

This work has been financially supported by Machinefabriek Kreber BV under a TU Delft/Kreber Research Agreement.

APPENDIX A: A NOTE ON THE DERIVATION OF THE SLENDER-JET MODEL IN THE PRESENCE OF MARANGONI STRESSES AND AMBIENT COOLING

Considering an axisymmetric jet, Eqs. (1b) and (1c) for the axial momentum balance and energy balance, respectively, read

$$\rho \left(\frac{\partial v}{\partial t} + u \frac{\partial v}{\partial r} + v \frac{\partial v}{\partial z} \right) = -\frac{\partial p}{\partial z} + \frac{1}{r} \frac{\partial}{\partial r} \left(r \eta(T) \frac{\partial v}{\partial r} \right) + \frac{\partial}{\partial z} \left(\eta(T) \frac{\partial v}{\partial z} \right), \quad (\text{A1a})$$

$$\rho c_p \left(\frac{\partial T}{\partial t} + u \frac{\partial T}{\partial r} + v \frac{\partial T}{\partial z} \right) = k_c \left(\frac{\partial^2 T}{\partial r^2} + \frac{1}{r} \frac{\partial T}{\partial r} + \frac{\partial^2 T}{\partial z^2} \right). \quad (\text{A1b})$$

At the jet free surface $r = R(z, t)$, the outward normal and tangential unit vectors are respectively given by

$$\mathbf{n} = \frac{1}{\sqrt{1+R'^2}} \begin{bmatrix} 1 \\ 0 \\ -R' \end{bmatrix}, \quad \mathbf{t} = \frac{1}{\sqrt{1+R'^2}} \begin{bmatrix} R' \\ 0 \\ 1 \end{bmatrix},$$

where $R' = \frac{\partial R}{\partial z}$. The dynamic and thermal interface conditions, Eqs. (2) and (5), respectively, can then be written as

$$p - \frac{2\eta(T)}{1+R'^2} \left[\frac{\partial u}{\partial r} - \left(\frac{\partial u}{\partial z} + \frac{\partial v}{\partial r} \right) R' + \frac{\partial v}{\partial z} R'^2 \right] = \gamma(T)\kappa, \quad (\text{A2a})$$

$$\frac{\eta(T)}{\sqrt{1+R'^2}} \left[2 \left(\frac{\partial u}{\partial r} - \frac{\partial v}{\partial z} \right) R' + \left(\frac{\partial v}{\partial r} + \frac{\partial u}{\partial z} \right) (1-R'^2) \right] = \frac{d\gamma}{dT} \left[R' \frac{\partial T}{\partial r} + \frac{\partial T}{\partial z} \right], \quad (\text{A2b})$$

$$-\frac{k_c}{\sqrt{1+R'^2}} \left(\frac{\partial T}{\partial r} - R' \frac{\partial T}{\partial z} \right) = h_w(T - T_\infty). \quad (\text{A2c})$$

Inserting the radial expansions given by Eq. (6) into Eqs. (A1) yields the following up to $O(r^2)$:

$$\rho \left(\frac{\partial v_0}{\partial t} + v_0 v_0' \right) = -p_0' + \eta(T)(4v_2 + v_0'') + 2 \frac{d\eta}{dT} T_0' v_0' + O(r^2), \quad (\text{A3a})$$

$$\rho c_p \left(\frac{\partial T_0}{\partial t} + v_0 T_0' \right) = k_c(4T_2 + T_0'') + O(r^2). \quad (\text{A3b})$$

Note that the next lowest order in Eqs. (A1) is $O(r^2)$; therefore Eqs. (A3) also capture the full equations at $O(r)$. In line with the procedure detailed in [12], the interface conditions (A2) can be used to eliminate the variables p_0 , v_2 , and T_2 . The normal stress condition (A2a) will yield up to $O(r^2)$,

$$p_0 + \eta(T)v_0' = \gamma(T)\kappa + O(r^2), \quad (\text{A4})$$

which can be used to eliminate p_0 in Eq. (A3a).

When it comes to eliminating v_2 and T_2 , there appears a peculiarity with the left- and right-hand sides being at seemingly different orders. The referee correctly underlines this peculiarity for the heat transfer condition at the interface, given in Eq. (A2c), but the same is also apparent in the tangential stress balance given in Eq. (A2b), and its justification is either overlooked or not explicitly provided in the works related to surfactant-laden breakup by Ambravaneswaran, Wee, Basaran, and others [31,33,45,46]. Up to $O(r^2)$ the tangential stress balance reduces to

$$\underbrace{\eta(T) \left(-3v_0' R' - \frac{1}{2} v_0'' R + 2v_2 R \right)}_{O(r)} = \frac{d\gamma}{dT} T_0' + O(r^2). \quad (\text{A5})$$

In the absence of a mechanism that induces a Marangoni stress (e.g., tangential temperature or surfactant gradients), the right-hand side of (A5) will vanish and an expression for v_2 is obtained without any inconsistencies with the order of terms. In the presence of Marangoni stresses, however, we require that $\partial\gamma/\partial z$ matches with the left-hand side of $O(r)$ for consistency and hence $\partial\gamma/\partial z$ (thus $d\gamma/dT$) should be sufficiently small. So if one proceeds with solving (A5) for v_2 one will arrive at

$$v_2 = \frac{1}{2\eta(T)R} \frac{d\gamma}{dT} \frac{\partial T}{\partial z} + \frac{3}{2} v_0' \frac{R'}{R} + \frac{v_0''}{4}. \quad (\text{A6})$$

This is precisely the expression used in [31,33,45,46] to close the 1D system as well as the works by Furlani and Hanchak, where they considered surface tension modulation at the inlet [47,48]. Note

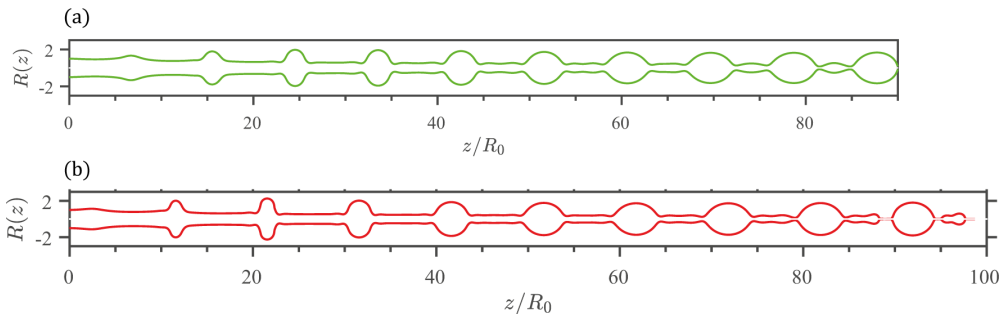


FIG. 9. Free surface profiles from our 1D model with the regularization scheme. Our results are in near perfect agreement with the 1D- and 2D-axisymmetric simulations shown in Fig. 11 of McIlroy and Harlen [44]. The model parameters are $We = 338$, $Oh = 0.122$, $kR_0 = 0.7$. The amplitude of velocity perturbations are (a) $\varepsilon_v = 0.1$ and (b) $\varepsilon_v = 0.15$. Shift from inverted pinching back to downstream pinching is reproduced with our code as well.

that in [47,48] the surface tension gradient is fixed, so there is no additional balance equation for the surfactant concentration or thermal energy.

Looking at the physical side, this approach implicitly assumes that the tangential stress difference at the interface caused by the Marangoni stress is not too large. In cases where the Marangoni stress is not small, then the slender-jet approach would not be useful, as the viscous boundary layer within jet due to the high tangential stress could not be captured [49].

Along similar lines, one could justify the same choice in the heat transfer boundary condition. Up to $O(r^2)$ the heat transfer boundary condition at the interface reduces to

$$\underbrace{-k_c(2T_2R - R'T_0')}_{O(r)} = h_w(T_0 - T_\infty) + O(r^2). \quad (\text{A7})$$

If we proceed with solving for T_2 , we get

$$T_2 = -\frac{h_w(T_0 - T_\infty)}{2k_cR} + \frac{T_0R'}{2R}. \quad (\text{A8})$$

This expression is also obtained and used in the studies by Pillai *et al.* [26], Furlani *et al.* [28], and several others concerning nonisothermal melt spinning processes [50,51]. This time the physical explanation is related to the thermal boundary layer, namely, if the cooling to the ambient is too large ($Bi \gg 1$), then a thermal boundary layer would arise within the jet, and the slender-jet approach would be unable to capture the radial variation of the temperature near the jet edge.

TABLE III. Tabulated comparison of the case described in Sec. 3.1 of Ref. [24].

	Bi = 0.1		Bi = 10	
	Mashayek & Ashgriz	Our code	Mashayek & Ashgriz	Our code
Breakup time, t_b	26.82	26.23	23.99	29.05
Main drop radius	1.878	1.878	1.862	1.856
Satellite drop radius	0.474	0.473	0.656	0.694

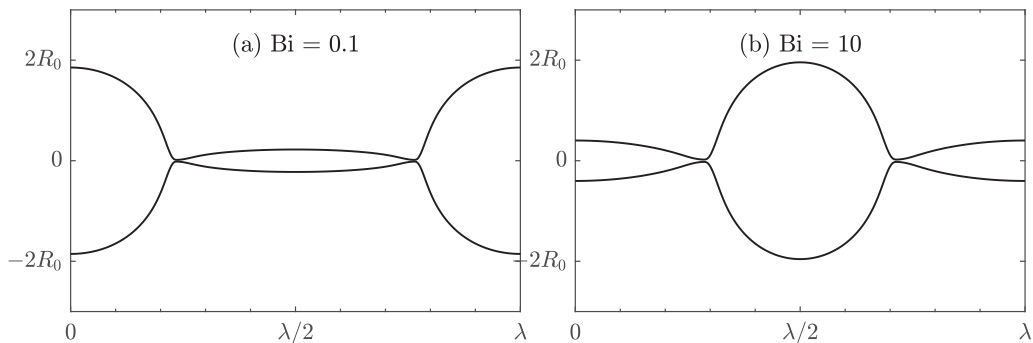


FIG. 10. Filament shapes from the case described in Sec. 3.1 of Ref. [24].

APPENDIX B: VALIDATION OF THE NUMERICAL MODEL

In this section we provide some comparison against full 2D-axisymmetric simulations in the field of nozzle-driven jet breakup and the breakup of periodic filaments in a moving frame of reference. In their recent study, McIlroy and Harlen [44] discussed the effect of the amplitude of velocity disturbances on the breakup characteristic of an isothermal jet. They observed a narrow window of amplitudes for which the filaments break up on the upstream end rather than the downstream end (i.e., inverted pinching). This phenomenon is also discussed in our present paper with respect to the amplitude of the thermal perturbation (see Sec. III B). A comparison with a full 2D-axisymmetric solution for certain cases is also provided in [44], so we chose this work as a relevant benchmark case to test our code. Figure 9 shows our results for the case described in Sec. C of Ref. [44]. Results are in very good agreement with the 1D- and 2D-axisymmetric results presented in [44]. The shift in the breakup characteristic from inverted pinching to downstream pinching is captured with our code as well.

In addition to this, we provide a comparison with respect to another full-axisymmetric simulation from the literature by Mashayek and Ashgriz [24], where they consider nonisothermal breakup of liquid jets. Specifically, we ran a few simulations for the case described in Sec. 3.1 of Ref. [24] and tabulate the results in Table III. While for low Biot number the agreement is excellent, for the high Biot numbers there is a discrepancy, which is due to the same reasons mentioned in Appendix A. Nevertheless, we were able to observe the shift from capillary breakup to thermocapillary breakup discussed in [24] (that happens around $Bi \approx 1.37$ according to their results) in between our cases, namely, $Bi = 0.1$ to $Bi = 10$. The resultant filament shapes for the two Biot numbers are shown in Fig. 10.

-
- [1] H. N. Chapman, P. Fromme, A. Barty, T. A. White, R. A. Kirian, A. Aquila, M. S. Hunter, J. Schulz, D. P. DePonte, U. Weierstall *et al.*, Femtosecond x-ray protein nanocrystallography, *Nature (London)* **470**, 73 (2011).
 - [2] M. O. Wiedorn, S. Awel, A. J. Morgan, K. Ayer, Y. Gevorkov, H. Fleckenstein, N. Roth, L. Adriano, R. Bean, K. R. Beyerlein *et al.*, Rapid sample delivery for megahertz serial crystallography at x-ray fells, *IUCrJ* **5**, 574 (2018).
 - [3] H. B. Eral, M. O'Mahony, R. Shaw, B. L. Trout, A. S. Myerson, and P. S. Doyle, Composite hydrogels laden with crystalline active pharmaceutical ingredients of controlled size and loading, *Chem. Mater.* **26**, 6213 (2014).
 - [4] H. B. Eral, E. R. Safai, B. Keshavarz, J. J. Kim, J. Lee, and P. S. Doyle, Governing principles of alginate microparticle synthesis with centrifugal forces, *Langmuir* **32**, 7198 (2016).

-
- [5] C. M. Van't Land, *Industrial Crystallization of Melts* (CRC Press, Boca Raton, FL, 2004).
- [6] L. Rayleigh, On the capillary phenomena of jets, *Proc. R. Soc. London* **29**, 71 (1879).
- [7] L. Rayleigh, On the instability of cylinder fluid surfaces, *Philos. Mag.* **34**, 145 (1892).
- [8] S. Chandrasekhar, *Hydrodynamic and Hydromagnetic Stability* (Courier Corporation, North Chelmsford, MA, 2013).
- [9] J. B. Keller, S. I. Rubinow, and Y. O. Tu, Spatial instability of a jet, *Phys. Fluids* **16**, 2052 (1973).
- [10] S. J. Leib and M. E. Goldstein, Convective and absolute instability of a viscous liquid jet, *Phys. Fluids* **29**, 952 (1986).
- [11] J. Eggers, Universal Pinching of 3D Axisymmetric Free-Surface Flow, *Phys. Rev. Lett.* **71**, 3458 (1993).
- [12] J. Eggers and T. F. Dupont, Drop formation in a one-dimensional approximation of the Navier–Stokes equation, *J. Fluid Mech.* **262**, 205 (1994).
- [13] J. Eggers, Nonlinear dynamics and breakup of free-surface flows, *Rev. Mod. Phys.* **69**, 865 (1997).
- [14] D. T. Papageorgiou, On the breakup of viscous liquid threads, *Phys. Fluids* **7**, 1529 (1995).
- [15] D. T. Papageorgiou, Analytical description of the breakup of liquid jets, *J. Fluid Mech.* **301**, 109 (1995).
- [16] E. D. Wilkes, S. D. Phillips, and O. A. Basaran, Computational and experimental analysis of dynamics of drop formation, *Phys. Fluids* **11**, 3577 (1999).
- [17] B. Ambravaneswaran, E. D. Wilkes, and O. A. Basaran, Drop formation from a capillary tube: Comparison of one-dimensional and two-dimensional analyses and occurrence of satellite drops, *Phys. Fluids* **14**, 2606 (2002).
- [18] F. J. García, H. González, J. R. Castrejón-Pita, and A. A. Castrejón-Pita, The breakup length of harmonically stimulated capillary jets, *Appl. Phys. Lett.* **105**, 094104 (2014).
- [19] T. Driessen, P. Sleutel, F. Dijkman, R. Jeurissen, and D. Lohse, Control of jet breakup by a superposition of two Rayleigh-plateau-unstable modes, *J. Fluid Mech.* **749**, 275 (2014).
- [20] B. Keshavarz, V. Sharma, E. C. Houze, M. R. Koerner, J. R. Moore, P. M. Cotts, P. Threlfall-Holmes, and G. H. McKinley, Studying the effects of elongational properties on atomization of weakly viscoelastic solutions using Rayleigh Ohnesorge jetting extensional rheometry (Rojer), *J. Non-Newtonian Fluid Mech.* **222**, 171 (2015).
- [21] O. A. Basaran, H. Gao, and P. P. Bhat, Nonstandard inkjets, *Annu. Rev. Fluid Mech.* **45**, 85 (2013).
- [22] J-J Xu and S. H. Davis, Instability of capillary jets with thermocapillarity, *J. Fluid Mech.* **161**, 1 (1985).
- [23] H. C. Kuhlmann and H. J. Rath, Hydrodynamic instabilities in cylindrical thermocapillary liquid bridges, *J. Fluid Mech.* **247**, 247 (1993).
- [24] F. Mashayek and N. Ashgriz, Nonlinear instability of liquid jets with thermocapillarity, *J. Fluid Mech.* **283**, 97 (1995).
- [25] Z. Gao and K. Ng, Thermal modulation and breakup of liquid jets, *Int. J. Numer. Methods Fluids* **70**, 326 (2012).
- [26] D. S. Pillai, P. Narayanan, S. Pushpavanam, T. Sundararajan, A. Jasmin Sudha, and P. Chellapandi, A nonlinear analysis of the effect of heat transfer on capillary jet instability, *Phys. Fluids* **24**, 124106 (2012).
- [27] R. W. Faidley and R. L. Panton, Measurement of liquid jet instability induced by surface tension variations, *Exp. Therm. Fluid Sci.* **3**, 383 (1990).
- [28] E. P. Furlani, B. G. Price, G. Hawkins, and A. G. Lopez, Thermally induced Marangoni instability of liquid microjets with application to continuous inkjet printing, in *Proceedings of the NSTI Nanotechnology Conference Trade Show* (Nano Science and Technology Institute, Austin, TX, 2006), Vol. 2, pp. 534–537.
- [29] J. M. Chwalek, D. P. Trauernicht, C. N. Delametter, R. Sharma, D. L. Jeanmaire, C. N. Anagnostopoulos, G. A. Hawkins, B. Ambravaneswaran, J. C. Panditaratne, and O. A. Basaran, A new method for deflecting liquid microjets, *Phys. Fluids* **14**, L37 (2002).
- [30] R. Suryo and O. A. Basaran, Dripping of a Liquid from a Tube in the Absence of Gravity, *Phys. Rev. Lett.* **96**, 034504 (2006).
- [31] B. Ambravaneswaran and O. A. Basaran, Effects of insoluble surfactants on the nonlinear deformation and breakup of stretching liquid bridges, *Phys. Fluids* **11**, 997 (1999).

- [32] P. M. Kamat, B. W. Wagoner, S. S. Thete, and O. A. Basaran, Role of Marangoni stress during breakup of surfactant-covered liquid threads: Reduced rates of thinning and microthread cascades, *Phys. Rev. Fluids* **3**, 043602 (2018).
- [33] H. Wee, B. W. Wagoner, P. M. Kamat, and O. A. Basaran, Effects of Surface Viscosity on Breakup of Viscous Threads, *Phys. Rev. Lett.* **124**, 204501 (2020).
- [34] I. Orlanski, A simple boundary condition for unbounded hyperbolic flows, *J. Comput. Phys.* **21**, 251 (1976).
- [35] B. Van Leer, Towards the ultimate conservative difference scheme. II. Monotonicity and conservation combined in a second-order scheme, *J. Comput. Phys.* **14**, 361 (1974).
- [36] T. Driessen and R. Jeurissen, A regularised one-dimensional drop formation and coalescence model using a total variation diminishing (TVD) scheme on a single Eulerian grid, *Int. J. Comput. Fluid Dyn.* **25**, 333 (2011).
- [37] C. Clasen, J. Eggers, M. A. Fontelos, J. Li, and G. H. McKinley, The beads-on-string structure of viscoelastic threads, *J. Fluid Mech.* **556**, 283 (2006).
- [38] A. Umemura, Self-stabilising loop of a low-speed water jet emanating from an orifice in microgravity, *J. Fluid Mech.* **797**, 146 (2016).
- [39] A. M. Ganán-Calvo, H. N. Chapman, M. Heymann, M. O. Wiedorn, J. Knoska, B. Gañán-Riesco, J. M. López-Herrera, F. Cruz-Mazo, M. A. Herrada, J. M. Montanero, and S. Bajt, The natural breakup length of a steady capillary jet: Application to serial femtosecond crystallography, *Crystals* **11**, 990 (2021).
- [40] S. Le Dizès and E. Villermaux, Capillary jet breakup by noise amplification, *J. Fluid Mech.* **810**, 281 (2017).
- [41] U. S. Sauter and H. W. Buggisch, Stability of initially slow viscous jets driven by gravity, *J. Fluid Mech.* **533**, 237 (2005).
- [42] J. Meessen and H. Petersen, *Urea, Uhlmann's Encyclopedia of Industrial Chemistry* (Wiley, New York, 2010).
- [43] W. T. Pimbley and H. C. Lee, Satellite droplet formation in a liquid jet, *IBM J. Res. Dev.* **21**, 21 (1977).
- [44] C. McIlroy and O. G. Harlen, Effects of drive amplitude on continuous jet break-up, *Phys. Fluids* **31**, 064104 (2019).
- [45] Y-C Liao, E. I. Franses, and O. A. Basaran, Deformation and breakup of a stretching liquid bridge covered with an insoluble surfactant monolayer, *Phys. Fluids* **18**, 022101 (2006).
- [46] H. Wee, B. W. Wagoner, V. Garg, P. M. Kamat, and O. A. Basaran, Pinch-off of a surfactant-covered jet, *J. Fluid Mech.* **908**, A38 (2021).
- [47] E. P. Furlani, Temporal instability of viscous liquid microjets with spatially varying surface tension, *J. Phys. A: Math. Gen.* **38**, 263 (2004).
- [48] E. P. Furlani and M. S. Hanchak, Nonlinear analysis of the deformation and breakup of viscous microjets using the method of lines, *Int. J. Numer. Methods Fluids* **65**, 563 (2011).
- [49] A. Martínez-Calvo, J. Rivero-Rodríguez, B. Scheid, and A. Sevilla, Natural break-up and satellite formation regimes of surfactant-laden liquid threads, *J. Fluid Mech.* **883**, A35 (2020).
- [50] K. Gupta and P. Chokshi, Stability analysis of non-isothermal fibre spinning of polymeric solutions, *J. Fluid Mech.* **851**, 573 (2018).
- [51] D. Deshwar and P. Chokshi, Stability analysis of a thinning electrified jet under nonisothermal conditions, *Phys. Rev. E* **103**, 023107 (2021).